Nanoscale

PAPER

View Article Online
View Journal | View Issue

Cite this: *Nanoscale*, 2017, **9**, 16446

Shell thickness effects on quantum dot brightness and energy transfer†

Margaret Chern,[a] Thuy T. Nguyen,[b] Andrew H. Mahler[b] and Allison M. Dennis *[b]

Heterostructured core/shell quantum dots (QDs) are prized in biomedical imaging and biosensing applications because of their bright, photostable emission and effectiveness as Förster resonance energy transfer (FRET) donors. However, as nanomaterials chemistry has progressed beyond traditional QDs to incorporate new compositions, ultra-thick shells, and alloyed structures, few of these materials have had their optical properties systematically characterized for effective application. For example, thick-shelled QDs, also known as 'giant' QDs (gQDs) are useful in single-particle tracking microscopy because of their reduced blinking, but we know only that CdSe/CdS gQDs are qualitatively brighter than thin-shelled CdSe/CdS in aqueous media. In this study, we quantify the impact of shell thickness on the nanoparticle molar extinction coefficient, quantum yield, brightness, and effectiveness as a FRET donor for CdSe/*x*CdS core/shell and CdSe/*x*CdS/ZnS core/shell/shell QDs, with variable thicknesses of the CdS shell (*x*). Molar extinction coefficients up to three orders of magnitude higher than conventional dyes and forty-fold greater than traditional QDs are reported. When thick CdS shells are combined with ZnS capping, quantum yields following thiol ligand exchange reach nearly 40%—5–10× higher than either the commercially available QDs or gQDs without ZnS caps treated the same way. These results clearly show that thick CdS shells and ZnS capping shells work in concert to provide the brightest possible CdSe-based QDs for bioimaging applications. We demonstrate that thicker shelled gQDs are over 50-fold brighter than their thin-shelled counterparts because of significant increases in their absorption cross-sections and higher quantum yield in aqueous milieu. Consistent with the point-dipole approximation commonly used for QD-FRET, these data show that thick shells contribute to the donor–acceptor distance, reducing FRET efficiency. Despite the reduction in FRET efficiency, even the thickest-shell gQDs exhibited energy transfer. Through this systematic study, we elucidate the tradeoffs between signal output, which is much higher for the gQDs, and FRET efficiency, which decreases with shell thickness. This study serves as a guide to nanobiotechnologists striving to use gQDs in imaging and sensing devices.

Received 15th June 2017,
Accepted 2nd October 2017

DOI: 10.1039/c7nr04296e

rsc.li/nanoscale

Introduction

Semiconductor quantum dots (QDs) have been used for nearly twenty years in biological imaging and sensing applications due to their brightness, high quantum yields, chemical robustness, and the versatility of the nanoparticle platform.[1–3] While the commercial availability of traditional CdSe/ZnS QDs makes the nanoparticles accessible for broad use, advances in QD chemistry beyond this standard composition provide further opportunities to tailor material properties to the application at hand. Alloyed, thick-shelled, and tertiary heterostructures each present a different approach to bandgap engineering,[4,5] reducing blinking due to charging and Auger recombination,[6,7] and brightness-matching of QD emissions at different colors.[8]

Thick-shelled QDs, also known as 'giant' nanocrystal quantum dots or gQDs, utilize up to 20 atomic monolayers of a second semiconductor epitaxially grown on the optically active core to function as a protective layer as well as affect the localization of the electron and hole in the exciton. Examples of thick-shelled QDs include the prototypical gQD comprising CdSe/CdS,[9,10] gQDs with an alloyed shell (CdSe/$Cd_xZn_{1-x}S$), the Type II near infrared emitter InP/CdS,[11] and cadmium-free varieties comprising InP/ZnSe.[12] Thorough investigations into ensemble and single-particle gQD optical properties have contributed to a deeper understanding of the blinking dynamics of semiconductor nanocrystals.[6,7,9,10,13–16]

The CdSe/CdS core/shell was chosen for our investigation because these well-established, thick-shelled heterostructures exhibit exceptional photophysical properties including

[a]*Division of Materials Science and Engineering, Boston University, Boston, Massachusetts, 02446, USA*
[b]*Department of Biomedical Engineering, Boston University, Boston, Massachusetts, 02446, USA. E-mail: aldennis@bu.edu*
†Electronic supplementary information (ESI) available. See DOI: 10.1039/c7nr04296e

reduced Auger recombination and suppressed blinking,[7,10,17] increased brightness due to large molar extinction coefficients,[8] and chemical robustness allowing for surface ligand transfer with a smaller reduction in quantum yield (QY).[7,8] Their non-blinking nature has been effectively applied in both solid state lighting applications[18] and single particle tracking microscopy.[19] Due to the small difference in the CdSe and CdS conduction band energies, the CdSe/*x*CdS heterostructure exhibits hole confinement in the core and spreading of the excited electron across the core and shell, yielding a quasi-type II bandgap alignment.[20,21] It was qualitatively shown that the thick-shelled CdSe/CdS QDs luminesce visibly in aqueous milieu following thiol-based ligand exchange, while thin-shelled CdSe/CdS QDs are quenched.[7] This result is not surprising given the (finite) spreading of the exciton probability function to the particle surface.[22] Traditional QDs (*i.e.*, non-thick-shelled CdSe) typically utilize a passivating shell of the high bandgap semiconductor ZnS to fully confine the exciton to the core before phase transfer to aqueous media for biomedical applications.[1] Here we systematically investigate the impact of the ZnS shell on quasi-type II CdSe/CdS QDs with various CdS shell thicknesses to assess the benefit of each shell in biological imaging and sensing applications.

In addition to the particle brightness in aqueous milieu, we examine the impact of the QD heterostructure on energy transfer. Förster resonance energy transfer (FRET) is a dipole–dipole interaction between fluorescent species that results in non-radiative energy transfer from a donor to acceptor molecule. FRET efficiency is inversely proportional to the donor–acceptor distance to the sixth power.[23] The strength of this dependence makes FRET a valuable tool for sensing nanometer scale changes in distance that may arise from conformational changes, biomolecular binding, or enzymatic cleavage.[24–28] QDs are effective FRET donors due to their excellent photostability, ability to bind multiple acceptors per donor, and broadband absorption.[1,27,29,30] The absorption profile of QDs enables photonic excitation of the FRET donor at wavelengths distinct from the acceptor absorption. This eliminates excitation cross talk, simplifying assay design and analysis. The optical versatility of QDs has resulted in their application in more exotic energy transfer schemes as well, including bioluminescence or chemiluminescence resonance energy transfer (BRET or CRET, respectively),[31,32] sensors utilizing QDs as fluorescent acceptors,[33] and multistep and/or time gated energy transfer devices.[34,35] The long list of sensors developed using QDs in energy transfer devices include measures of the environment like pH[36–38] or O_2 saturation,[39] enzymatic cleavage,[28,40–44] DNA hybridization,[45–47] label-free detection of small molecule analytes or microRNA,[48,49] and immunoassays.[50,51]

While the increased quantum yields of thick-shelled QD donors increases the spectral overlap integral of the donor–acceptor pair, thereby lengthening the Förster distance for the QD-acceptor system, increasing donor radius increases the distance between donor and acceptor molecules and decreases FRET efficiency (E_{FRET}). Our systematic analysis shows the advantages and disadvantages of using gQDs in aqueous media and particularly as FRET donors in biomedical applications.

Results and discussion

Impact of shells on QD brightness

A systematic series of core/shell and core/shell/shell quantum dots were synthesized to determine the effect of CdS shell thickness and ZnS capping on QD properties. CdS shells of various thicknesses were deposited onto CdSe cores using a modified successive ion layer adsorption and reaction (SILAR) procedure.[17,52] SILAR is used to add the cationic and anionic shell precursors independently with subsequent high temperature anneals in order to promote shell growth and avoid nucleation of the shell semiconductor. The added precursor amounts are sufficient for a single monolayer of shell deposition with each round of SILAR, allowing for our controlled shell thickness study. Six CdS shell thicknesses were produced in individual flasks through 1, 4, 7, 10, 13, and 16 rounds of shell deposition. Following CdS shelling, a significant sample of the CdSe/*x*CdS core/shell was collected before remaining particles were further capped with ZnS through two additional rounds of SILAR. Each of the twelve samples evaluated (six CdS shell thicknesses, with and without the ZnS cap) were imaged with transmission electron microscopy (TEM) (Fig. 1) and the images analyzed for size and morphology. Outlines were drawn around 109–535 particles per sample and their areas determined. The particle diameters were estimated by calculating the diameter of a circle with the same area as the outlined particles. While both the CdSe/*x*CdS core/shell particles and the CdSe/*x*CdS/2ZnS exhibited size dispersions of 7–12% (Table 1), the average size distribution was slightly higher for the ZnS capped QDs (9.8 ± 1.3% *vs.* 8.5 ± 1.7%).

The surface of as-synthesized QDs is coated with hydrocarbon-based coordinating ligands. Before these hydrophobic nanomaterials can be used for biologically relevant applications, they must be rendered water-soluble through the addition of an amphiphilic coating or ligand exchange to impart a hydrophilic colloidal corona. We chose a zwitterionic, bidentate thiolate dubbed CL4 ('compact ligand 4'; 3,3′-((2-(6,8-dimercaptooctanamido)ethyl)azanediyl)dipropionic acid) to phase exchange the QDs to ensure small particle size, colloidal stability, and access to the QD surface for biomolecular self-assembly (Scheme 1).[53] Traditional QDs have been shown to suffer significant loss in quantum yield (QY) after ligand exchange with thiol-based ligands when compared to amphiphilic polymer or lipid-PEG coatings that do not bind directly to the inorganic particle surface.[1,54] Surface passivation with a wider bandgap material, typically ZnS, is needed for traditional QDs to exhibit photoluminescence (PL) in aqueous media. We measured the PL and relative quantum yields of all twelve core/shell and core/shell/shell nanoparticles in hexane and in water following ligand exchange with CL4 to quantify the impact that the thick CdS shell and ZnS cap had on QD

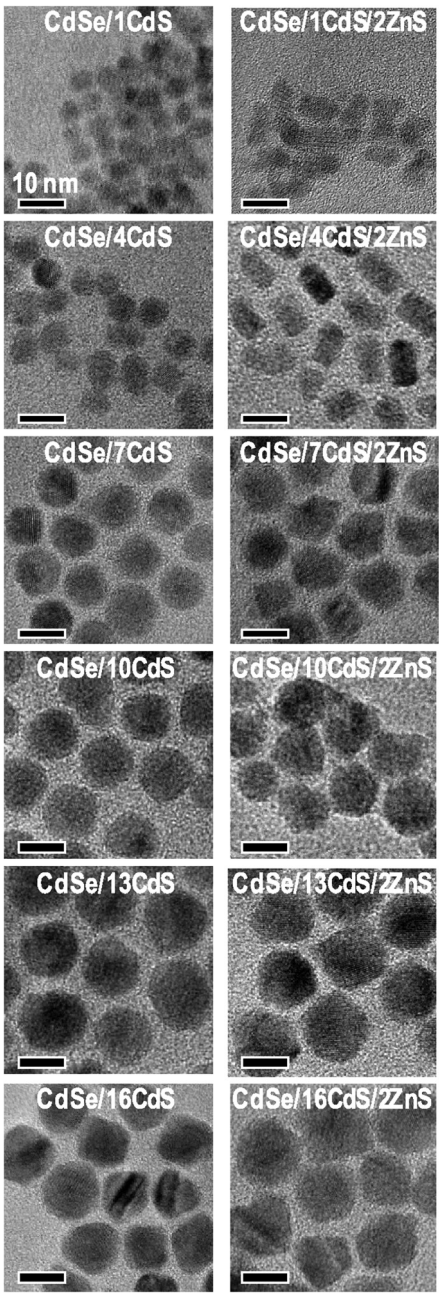

Fig. 1 Representative TEM images of core/shell and core/shell/shell QDs. The same CdSe core particles were used for all reactions with variable numbers of SILAR additions of CdS and ZnS shell layers. The numbers in the sample names indicate the number of SILAR reaction iterations and nominal number of monolayers of shell semiconductor added. Scale bar indicates 10 nm in all images.

emission. The CdS shelling induced a redshift in the PL emission peak that increased with thicker shells until stabilizing around 630 nm (Fig. S1†). The ZnS cap resulted in nominal red- or blue-shifting of the PL peak position, but significantly increased the full width half max (FWHM) of the PL peak from 26 ± 1 to 36 ± 6 ($p < 0.05$) (Table 1).

The photoluminescence decay of each of the QD samples was measured in both hexane and water. For the core/shell samples, lifetime increased slightly with QD size/shell thickness because of the Quasi-Type II bandstructure of CdSe/CdS (Fig. S2†). The conduction band offset for this system is low, and the electron probability density spreads into the shell, reducing the electron–hole overlap. The increase in lifetime plateaued for the thicker shells (10–16 CdS), indicating that the decrease in electron confinement no longer significantly impacts its probability distribution. This correlates with minimal red-shift between samples with 10 or more CdS monolayers (Fig. S1†). Samples that have been ligand exchanged or that include ZnS caps follow a similar trend, but less uniformly. The addition of a third semiconductor increases the PL lifetime, but variably, as the efficiency of ZnS shelling varies between samples (Table 1) and the behavior of the electron probability density is less well defined. For samples that have undergone ligand exchange, the surface of the QDs have been disrupted, possibly resulting in the creation of surface traps that affect the QD fluorescent lifetimes.

The QY of the QDs in organic phase (Fig. 2A) first increases, then decreases, as a function of shell size. This is not unexpected: semiconductor shells are known to have a protective/passivating effect leading to the initial increase in QY, while thick shells increase the chances of defects, crystal lattice strain effects, and further spatial separation of the electron and hole.[7,17] The QY of commercial Qdot® 655 ITK™ organic quantum dots (ITK655) was measured for comparison. All QYs reported in this work are taken relative to Rhodamine 6G (R6G) in ethanol.

Most biologically relevant events occur in aqueous solution, and thus the performance of QD-based sensors depends on their optical properties in water. Traditional amphiphilic polymer coatings are bulky and thick, precluding histidine tag-mediated self-assembly as a mechanism for bioconjugation.[1,49,56] The use of shorter DHLA-based ligands allows for His-tag binding, but is often met with significant decreases in QY.[54] In the case of our CdSe/*x*CdS QDs, adding only 1 or 4 monolayers of CdS was not sufficiently protective in the face of the dative binding of thiols, and emission intensity was completely lost (Fig. 2B). QDs with 7 or more CdS monolayers exhibit measurable QYs following ligand transfer, but at all shell thicknesses, the addition of the ZnS cap significantly increases the relative QY of the QD heterostructure ($p < 0.005$). The commercially available ITK655 are capped with ZnS and are most comparable to the CdSe/1CdS/2ZnS samples. CdSe/CdS with 7 and 10 CdS shell monolayers exhibit QYs in water comparable to ITK655 even without the ZnS cap. Moderate and thick CdS shells (7–16 shell monolayers) combined with ZnS caps greatly enhanced the relative QYs of the QDs following thiol-based ligand exchange with CL4, including compared to the ITK655 ($p < 0.001$). Core/shell/shell gQDs exhibited relative QYs of nearly 40% in water following thiol ligand exchange, demonstrating the importance of both the thick CdS shell and the ZnS cap to maximizing high QYs. Additional protective measures described in the literature like anaerobic exchange conditions[57] and/or photoligation protocols[58] may further preserve the pre-ligation QD emission intensities.

Table 1 Summary of QD properties

Sample	Diameter[a] (nm)	Shell thickness[b] (MLs)	ε_{400} [c] (10^6 M^{-1} cm^{-1})	Hydrodynamic diameter[d] (nm)	PL peak position (FWHM)[e] (nm)	PL lifetime[f] (ns)
CdSe	3.9 ± 0.3 (8%)	—	0.36[g]	—	570 (26)	—
CdSe/1CdS	4.8 ± 0.4 (8%)	1.3 CdS	0.59	6.9 ± 1.2	592 (27)	—
CdSe/1CdS/2ZnS	4.9 ± 0.5 (10%)	+0.2 ZnS		7.1 ± 0.3	613 (41)	13.3 ± 0.7
CdSe/4CdS	6.9 ± 0.5 (7%)	4.4 CdS	2.09	10.9 ± 1.2	614 (26)	—
CdSe/4CdS/2ZnS	8.1 ± 0.8 (10%)	+2.2 ZnS		11.7 ± 1.3	619 (39)	13.0 ± 0.8
CdSe/7CdS	8.8 ± 0.6 (7%)	7.2 CdS	4.17	10.8 ± 1.2	624 (26)	8.6 ± 0.7
CdSe/7CdS/2ZnS	10.0 ± 0.7 (7%)	+2.2 ZnS		13.3 ± 1.1	630 (43)	29.1 ± 1.2
CdSe/10CdS	11.7 ± 0.9 (9%)	12.0 CdS	8.74	12.9 ± 0.8	631 (28)	13.4 ± 0.8
CdSe/10CdS/2ZnS	12.4 ± 1.4 (11%)	+1.4 ZnS		16.5 ± 2.2	628 (34)	30.5 ± 1.0
CdSe/13CdS	12.8 ± 1.5 (12%)	13.2 CdS	13.97	14.4 ± 1.0	632 (25)	13.5 ± 0.6
CdSe/13CdS/2ZnS	14.2 ± 1.4 (10%)	+2.6 ZnS		18.2 ± 0.9	627 (29)	26.0 ± 0.9
CdSe/16CdS	15.4 ± 1.3 (8%)	17.0 CdS	22.55	19.7 ± 1.0	634 (26)	18.6 ± 1.0
CdSe/16CdS/2ZnS	16.7 ± 1.8 (11%)	+2.4 ZnS		20.3 ± 1.5	630 (28)	26.7 ± 1.0

[a] Particle diameter of core/shell and core/shell/shell determined with TEM image analysis. Average ± standard deviation (percent deviation) of 109–535 measurements. [b] Shell thicknesses determined from TEM-based diameter measurements reported in atomic monolayers (MLs) using monolayer thicknesses of 0.337 nm and 0.271 nm for wurtzite CdS and zinc blende ZnS, respectively. [c] Measured molar extinction coefficients of CdSe/*x*CdS QDs in chloroform at 400 nm. Values are nominally the same with and without the ZnS cap, as ZnS does not absorb at this wavelength. [d] Hydrodynamic diameter determined with dynamic light scattering (DLS) measurements taken in water after ligand transfer with CL4. Number weighted average is reported using particle refractive index of 1.6. Mean ± standard deviation of 5–10 measurements. [e] Full width at half maximum of the quantum dot spectra. [f] Reported PL lifetimes based on an amplitude-weighted average from a tri-exponential fit of the ligand-exchanged samples in aqueous media. Lifetimes are not listed for the CdSe, CdSe/1CdS, and CdSe/4CdSe samples because they are non-emissive following ligand exchange. [g] Extinction coefficient for CdSe core calculated using previously published empirical fit formulas[55] and used in conjunction with absorption spectra to calculate the extinction coefficient at 400 nm.

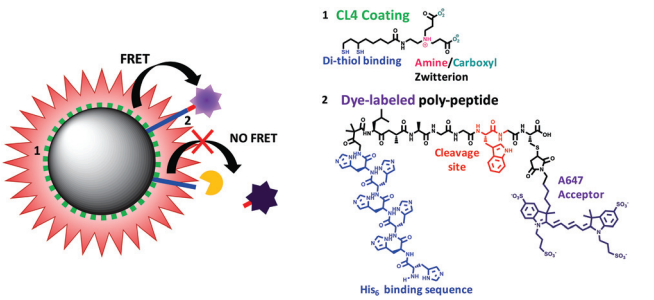

Scheme 1 Left: Schematic of the QD/A647 enzyme cleavage sensor. Right: Chemical structure of (1) compact ligand 4 (CL4) used to water solubilize the QDs and (2) the his-tagged, dye-labelled peptide. Structures drawn using ChemDraw.

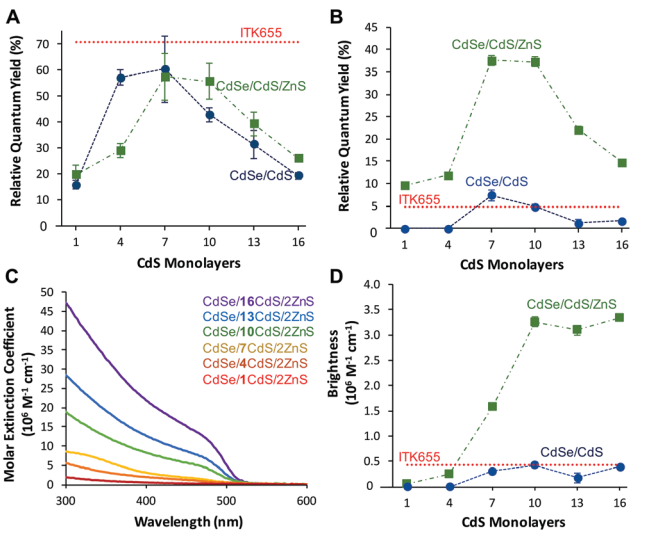

Fig. 2 Relative quantum yield (QY) of core/shells (blue circles) and core/shell/shells (green squares) (A) in hexane and (B) in water following ligand exchange, compared to commercially available ITK655 QDs before and after ligand transfer (horizontal red dotted lines). (C) Molar extinction coefficient as a function of wavelength for particles with increasing CdS shell thickness. (D) Relative brightness of core/shell (blue circles) and core/shell/shell (green squares) QDs in water with excitation at 400 nm, compared to commercially available ITK665 QDs (horizontal red line).

To assess the impact of the CdS shell thickness and the ZnS cap on the overall brightness of the heterostructured QDs, the molar extinction cross-section is needed in addition to the QY. The additional CdS shells have a direct impact on the molar extinction coefficient of the nanoparticles at wavelengths below 540 nm, the bulk bandgap of CdS, as there is more semiconductor material per QD to absorb. Known quantities and concentrations of the SILAR reaction solutions were diluted in chloroform and their absorbances measured to extract the particle molar extinction coefficients using the Beer–Lambert Law (Fig. 2C).[8] The absorptivity of ZnS is assumed to be negligible in the wavelength range of interest because the bulk bandgap of its hexagonal crystal is 3.9 eV (317 nm),[59] and is therefore excluded from consideration. The QDs described here range from 4 to 17 nm in diameter and thus exhibit large differences in the volume of optically absorp-

tive material per particle. The molar extinction coefficients from 300–500 nm are over an order of magnitude higher for the 16-shell gQDs than for the 1-shell CdSe/CdS.

The brightness of a fluorophore is determined by how much incident light it absorbs and the efficiency at which it converts the absorbed light into emitted light, *i.e.*, its molar extinction coefficient at the excitation wavelength multiplied by its QY.[8] As a result of increased molar extinction coefficients and high quantum yield, the brightness is exceptionally high for the CdSe/10CdS/ZnS sample. The 13 and 16 CdS shell samples maintain that level of brightness due to the increase in their molar extinction coefficients despite a notable decrease in their relative quantum yields (Fig. 2D). The brightness of each of the three thickest shelled samples (10, 13, 16) is an order of magnitude higher than that of the commercial QD treated with the same ligand-transfer protocol. This high level of brightness would be advantageous for imaging applications.

On brightness alone, there appears to be no advantage to increasing the CdS shell thickness beyond 10 shells. It has been well documented, however, that thicker-shelled gQDs exhibit less fluorescence intermittency (or blinking), which could be extremely helpful for single particle tracking microscopy. In Ghosh, *et al.*, a lower particle volume threshold of 750 nm^3 for CdSe/*x*CdS was described as necessary to observe a non-blinking fraction of gQDs, with larger non-blinking fractions emerging with further increases in the particle volume.[17] The CdSe/10CdS particles described here are just above that threshold volume (905 ± 250 nm^3), so may present a small fraction of non-blinking particles. This population fraction is expected to increase with increased shelling thickness, as previously described,[17] indicating that there may be applications where added shells are valuable for reasons other than brightness. A previous study[60] reports the effect of blinking on energy transfer. Generally speaking, the donor must be in an "on" state in order for energy transfer to occur.[60] It would follow that an increased non-blinking fraction of donor QDs would affect the overall energy transfer kinetics. Fluorescence intermittency, however, is unresolvable when using techniques that rely on ensemble averaging. In our studies, all of our measurements are performed on ensembles of QDs in solution, and therefore the effect of blinking on energy transfer was not explored.

FRET with gQD donors

QDs are known to be effective FRET donors because of their brightness, broad absorption and narrow, tunable emission, and the nanoparticle scaffold structure they provide a FRET device. Because of the strong dependence between the donor–acceptor distance and FRET efficiency, it is logical to expect thick-shelled gQDs to exhibit decreased energy transfer compared to thin-shelled QDs. Gains in QD QY and brightness, however, could offset some of the impact of the increase in donor–acceptor distance by increasing the Förster distance (R_0) and sensor signal, respectively. To study the impact of the thicker shells on FRET efficiency, QDs comprising each of the six shell thicknesses (1, 4, 7, 10, 13, and 16 monolayers of CdS) and a ZnS cap were tested in a FRET assay. CdSe/CdS QDs without the ZnS cap were omitted from the FRET assays due to a relative lack of brightness in aqueous media, particularly with thin shells.

All six of the core/shell/shell QDs used in the FRET assays exhibited PL peaks between 592 and 634 nm (Fig. S1†), enabling the use of a single fluorescent dye acceptor, Alexa Fluor 647 (AF647), for the series of experiments. Alexa Fluor® 647 C_2 Maleimide (ThermoFisher Scientific) was conjugated to a 6His-tagged peptide containing a C-terminal cysteine, facilitating His-tag mediated self-assembly to the QD surface. Previous work has demonstrated that His-tag binding is high affinity and stoichiometric with a Poissonian distribution of peptides per QD.[61] Our FRET analysis used the molar ratios of acceptor to donor as each sample was prepared and incorporated the Poissonian distribution into our calculations as has been previously described (eqn (6)).[43,62] Donor QDs were incubated with 0–10× dye-labeled peptide in 384 well plates for efficient measurement of replicates in a plate reader accessory to a Horiba NanoLog fluorimeter. Representative thin (1), medium (7), and thick (13) FRET spectra are shown in Fig. 3 while the remaining FRET assays (4, 10, and 16 shells) are shown in Fig. S5.† Energy transfer from the thin-shelled QDs to the AF647 dye is clearly exhibited by the decrease in the QD emission peak (610–630 nm) and increase in the AF647 emission at 668 nm (Fig. 3A–C). For the thinnest shelled QDs, oversaturation of the dye-labeled peptides resulted in red-shift and quenching of acceptor emission (Fig. S6†). We hypothesize that this is caused by over-crowding of dyes on the particle surface resulting in acceptor-acceptor energy transfer. Plots of FRET spectra shown in Fig. 3 include only the acceptor/donor ratios that do not exhibit this behavior; the remaining spectra can be found in Fig. S6.† The evidence of FRET is still very clear with the medium shelled donor, although less pronounced. The thick-shelled QDs exhibit the lowest amount of energy transfer (Fig. 3C), but there is still ~30% quenching of the QD with high peptide-dye ratios (Table 2).

While the thicker-shelled QDs exhibit much higher emission intensities than the thin-shelled QDs, close inspection shows a mismatch between the trends for maximum signal intensity seen in the FRET assays and the shell thickness-dependent QD brightness values presented in Fig. 2D. This is due to the non-linearity of PL intensity as a function of concentration even at rather dilute concentrations (tens of nM), especially for the 10, 13 and 16 shell QD donors (Fig. S3†).

Donor quenching is shown in comparison to collisional controls that included QDs and AF647 in the absence of His-tagged peptide (Fig. 3D). Collisional quenching is known to quench linearly as a function of concentration;[63] in contrast, the FRET data exhibits non-linear quenching described by the Hill equation that models binding events.[64] It has been shown that His-tag binding can increase the QD emission of unevenly coated particles by filling in surface defects.[29,54] PL enhancement was assessed for each of our QD donors by mixing QDs

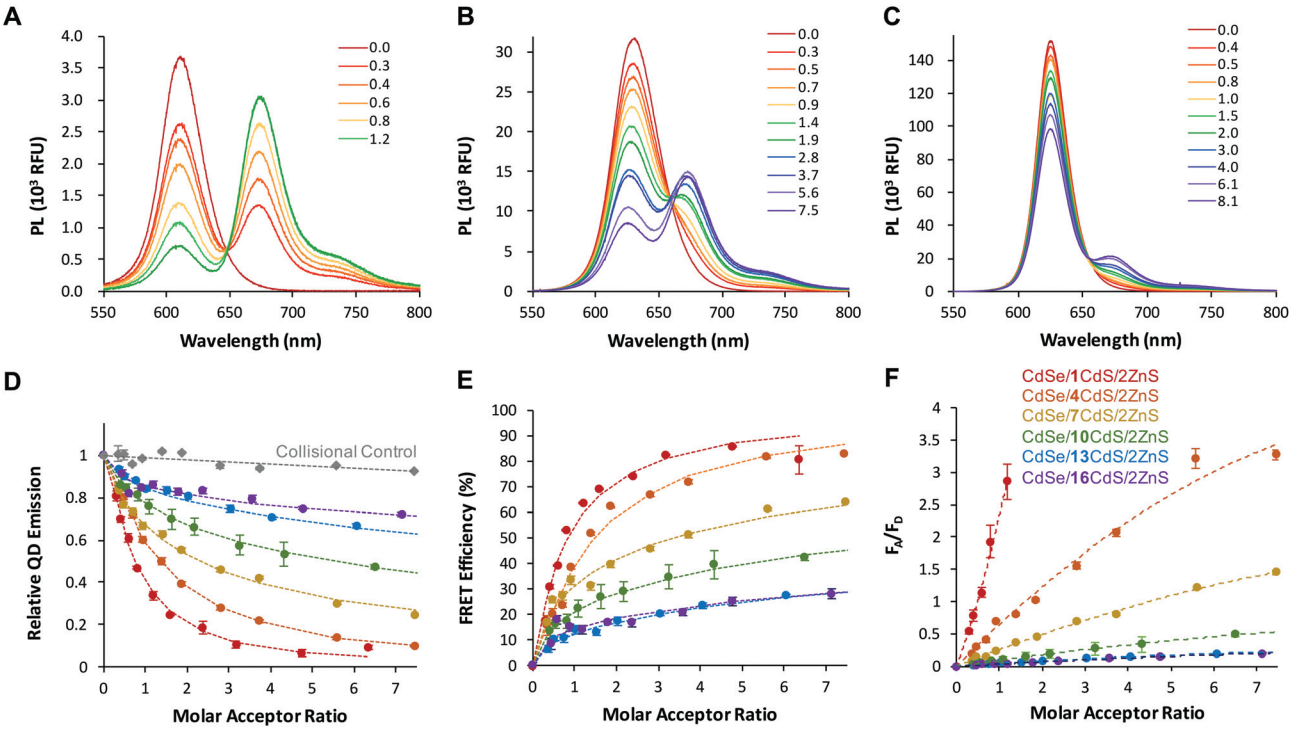

Fig. 3 Photoluminescence spectroscopy of FRET between QD donors and dye-labeled peptide acceptors using core/shell/shell nanoparticles donors with (A) thin, (B) medium, or (C) thick CdS shells. Specifically, these assays were performed with core/shell/shell QDs with 1, 7, or 13 CdS shell layers; the remaining spectra are presented in the ESI.† The legend refers to the number of AF647 acceptor dyes per QD donor. All spectra were background subtracted for direct acceptor excitation and averaged across triplicates. (D) Donor quenching *versus* the number of acceptors per donor for all shell thicknesses as well as a representative collisional quenching control. Plot (A) shows data up to a 1.2× molar ratio of acceptor for the sake of clarity; the corresponding donor quenching plot (D) shows data up to a 7.5× molar acceptor ratio; the full set of spectra can be found in the ESI.† (E) FRET efficiency (E_{FRET}) as a function of the number of acceptors bound. (F) Ratio of acceptor fluorescence to donor fluorescence (F_A/F_D) as a function of the number of acceptors bound. Data are means ± standard deviations of samples in triplicate with error propagation used where appropriate.

Table 2 FRET characteristics/results

Acceptor[a]	Absorption max (nm)		Extinction coefficient (M^{-1} cm^{-1})	
Alexa Fluor® 647	651		257 000	
Donor	J ($\times 10^{16}$ M^{-1} cm^{-1} nm^4)	R_0 (nm)	R_{DA} (nm)	E_{max} (n)[b]
CdSe/1CdS/2ZnS	1.55	5.50	3.88 ± 0.19	0.64 (1.2)
CdSe/4CdS/2ZnS	1.99	5.94	5.91 ± 0.44	0.67 (2.8)
CdSe/7CdS/2ZnS	2.39	7.43	9.00 ± 0.38	0.61 (5.6)
CdSe/10CdS/2ZnS	2.35	7.40	10.80 ± 0.84	0.46 (8.7)
CdSe/13CdS/2ZnS	2.24	6.73	11.10 ± 1.04	0.28 (8.1)
CdSe/16CdS/2ZnS	2.31	6.33	10.30 ± 0.93	0.33 (9.5)

[a] Alex Fluor® 647 characteristics taken from the specifications given by Life Sciences, Lot # 1764051. [b] Number of acceptors per donor at which maximum efficiency is reached. For donors with 1 and 4 CdS monolayers efficiency is listed for smallest n that does not exhibit acceptor–acceptor quenching.

and unlabeled His-tag peptides at concentrations equivalent to those for the QD and labeled His-tags in the FRET assays. For the QDs used in our assays, no enhancement was observed (Fig. S8†). Characteristics of the FRET pairs and experimentally obtained FRET results are reported in Table 2. Förster distance (R_0) is the distance at which FRET efficiency (E_{FRET}) is 50% and is a function of the degree of donor emission and acceptor absorption overlap, or overlap integral (J) (eqn (3) and (4)). As R_0 is dependent on donor QY, increasing donor QY increases the Förster distance of a FRET pair. In theory, if the increase in R_0 were larger than the increase in QD size, then the decrease in E_{FRET} due to large donor size may be overcome by the increase in donor QY. The gQDs did not maintain a high enough QY after thiol-based ligand transfer to fully overcome the increase in R_{DA}, but the higher QY (compared to thin-shelled QDs in this study) does help mitigate the impact of the increase in R_{DA}.

While FRET efficiency (Fig. 3E) is calculated solely using the donor emission, the ratiometric characteristic of FRET systems utilizing a fluorescent acceptor can be analyzed by plotting F_A/F_D (Fig. 3F), where F_A is fluorescence intensity of the acceptor in the presence of a donor and F_D is the fluorescence intensity of the donor in the presence of an acceptor. F_A/F_D describes the ratio of the donor and acceptor emission intensities and can be used to characterize an unknown sample if an initial calibration curve is generated. While generation of a calibration curve is necessary, ratiometric sensing is

sensor concentration independent and thus more reliable in complex sensing scenarios than single-color FRET-based sensors. Both the largest maximum efficiency and greatest range in F_A/F_D was achieved using the thinnest shelled donor (CdSe/1CdS/2ZnS). The signal intensity obtained from this assay, however, is ~50 times lower than that obtained from the assay using the CdSe/10CdS/2ZnS donor. To match signal intensities, the concentrations of donors and acceptors needed in a thin-shelled QD FRET system is much higher than those needed in assays that use gQDs. The CdSe/1CdS/2ZnS QDs need ~0.6 acceptors per donor to achieve ~50% E_{FRET}. Table 1 shows that the CdSe/10CdS/2ZnS QD achieves ~50% E_{FRET} at a ~1 : 6 ratio. To produce the same signal output as a QD with 10 CdS MLs, the smaller QD must be used at a concentration ~50× that of the gQD. This means that the gQD FRET assay can experience 50% E_{FRET} with the addition of ~5× less acceptor. In addition, high signal intensities would be beneficial in visual sensors where quick color-metric changes are preferred over measurements requiring expensive and/or complex instruments. If instrumentation is sensitive and E_{FRET} is the main concern, use of traditional QDs is preferable; if high and easily discernable signal output is the greater concern, then thick-shelled gQDs may provide an advantage.

Energy transfer was furthermore confirmed through our observation of a decrease in the fluorescence lifetime of the QD donors in the presence of the acceptors. Small, medium and large donors were added to a cuvette with PBS, pH 7.4 + 1% (w/v) BSA, at a final concentration of 25 nM. PL lifetime was monitored during titration of his-tagged AF647. The PL decays were plotted and curve fit to extract an amplitude-weighted average lifetime for each FRET condition (eqn (1) and (2)). These average lifetimes were used to quantify the FRET efficiency in each system. The FRET efficiencies obtained from the lifetime measurements was slightly lower than those calculated from the spectral results, but the same trend of decreasing FRET efficiency with thicker CdS shells was seen (Fig. 4). Semi-log plots of the lifetime measurements along with the individual fit components obtained can be found in Fig. S9 and Table S2† respectively.

Using gQDs in a FRET-based enzyme assay

A sensor for enzymatic proteolysis was developed to test the impact of the gQD shell thickness in a functional assay. Similar to previous QD-based cleavage assays,[43,65] the histidine tagged peptide sequence used to bind the AF647 dye to the QDs was specifically chosen such that the addition of α-Chymotrypsin cleaves the peptide linker, releasing the AF647 acceptor from the particle. The disassociation of the acceptor from the donor increases the donor–acceptor distance, thereby decreasing the FRET efficiency (Scheme 1). This is seen spectroscopically as a decrease in the sensitized acceptor emission and an increase in the donor PL (Fig. 5).

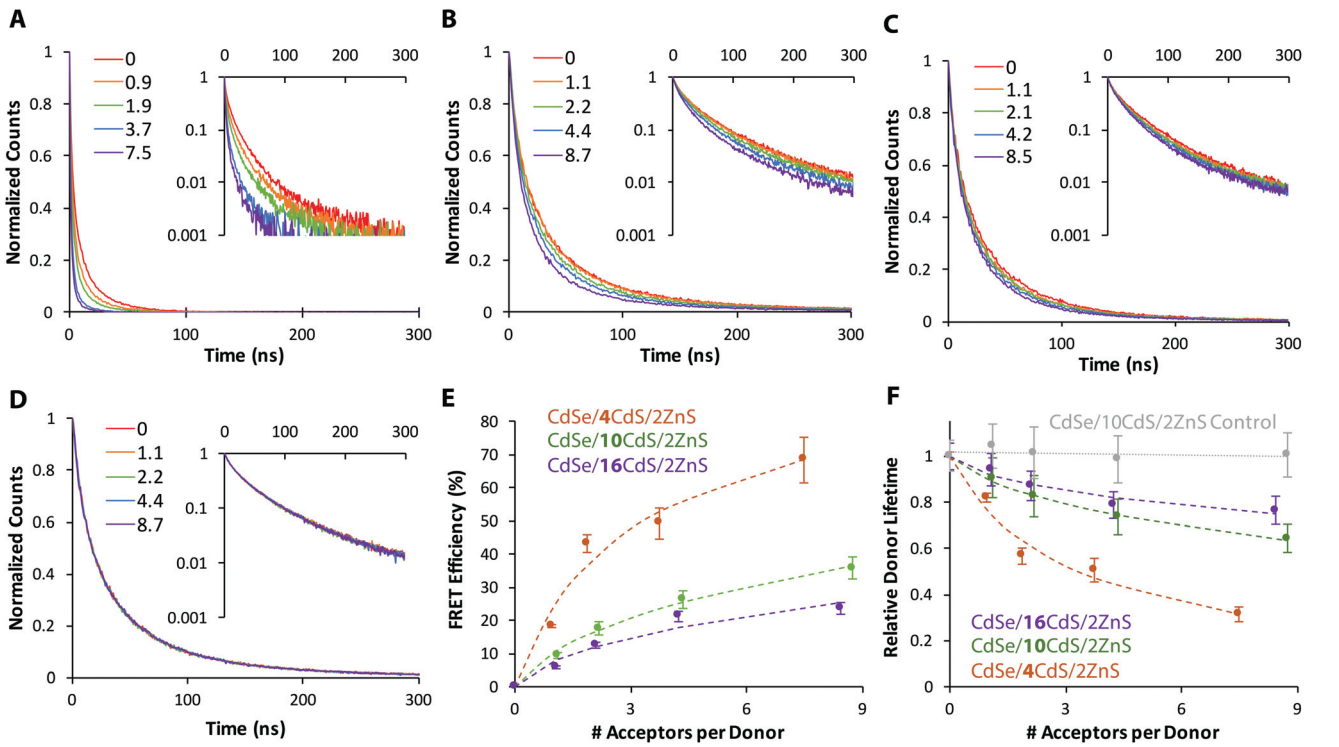

Fig. 4 PL decay spectra of (A) CdSe/4CdS/2ZnS, (B) CdSe/10CdS/2ZnS, and (C) CdSe/16CdS/2ZnS donors in the presence of his-tagged AF647. (D) A representative control experiment plotting the PL decay of a CdSe/10CdS/2ZnS donor in the presence of non his-tagged AF647. Inset plots are of the same data on a semi-log scale. The FRET efficiency (*E*) and decrease in donor lifetime (*F*) obtained from A, B and C. The error of each term, τ_i or A_i, in the tri-exponential fits of plots A–C were taken and used to determine the error bars in subplots E and F through standard error propagation techniques.

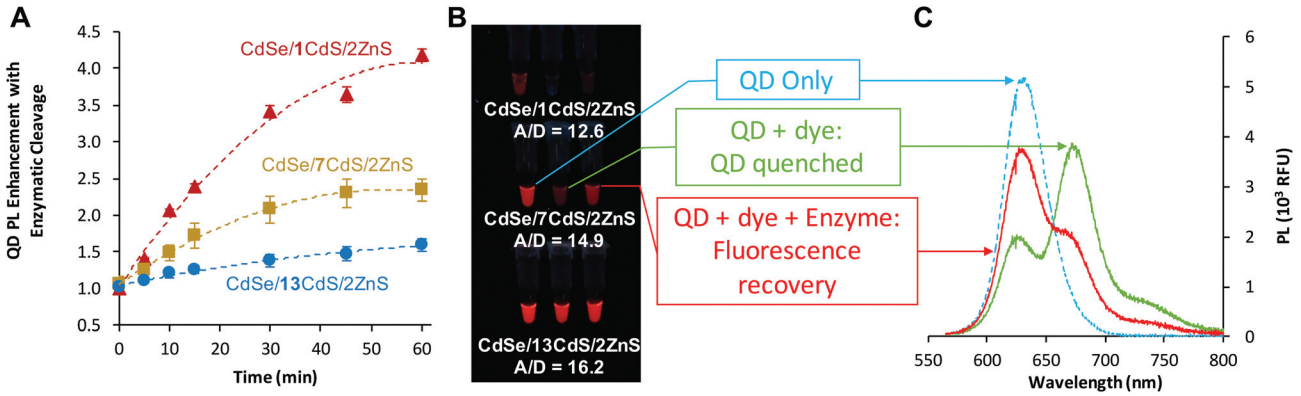

Fig. 5 (A) QD emission recovery after enzyme addition over time. Data is normalized to PL intensity at corresponding time points of the sensor after addition of buffer without enzyme present. Plots are of means ± standard deviations of triplicates. (B) Comparison of visual sensors for different QD donors at the QD concentrations used in Fig. 3 and acceptor/donor ratios as noted. Top to bottom: thin, medium and thick shelled donors. Left to right: QD only, QD A647 FRET quenching, QD + A647 + enzyme. (C) PL of the CdSe/7CdS/2ZnS sensor in the presence of enzyme (red) or buffer (green) compared to the QD control (dotted blue) after 30 minutes.

Because all of the QDs provide sufficient signal intensity when measured on a fluorimeter, the significantly higher FRET efficiency and range in F_A/F_D make the thin shelled QDs a better choice for spectrally resolved FRET sensors. For a larger gQD donor, increasing the number of acceptors per donor increases the range of F_A/F_D. This range, however, is somewhat limited when compared to thin-shelled QDs. gQD brightness is much brighter than the dye acceptor, so even at similar FRET efficiencies, the F_A/F_D for sensors utilizing a thin shelled donor is larger. Instead, we explore a way to exploit the brightness of the thick shelled donors by testing the possibility of using them in visual sensors. Visual read-outs are particularly relevant for point-of-care (POC) diagnostics and where a digital yes/no result is informative.

To make visual enzyme sensors, FRET conjugates using thin, medium, and thick shelled donors (1, 7, and 13 CdS shells, respectively) were loaded into 200 μL PCR tubes. Enzyme was added in excess (1 nmol) to each sensor and the difference between the different sensors was visually observed under illumination with a 365 nm ultraviolet light. QD-only tubes and QD + peptide-dye (FRET quenched) tubes were included for comparison. In the top row of Fig. 4B, the thin-shell QD emission in the left-most tube is nearly completely quenched by the presence of the dye-labeled peptide (middle tube). In the right-hand tube, there is QD brightening due to enzymatic cleavage of the dye-labeled peptide, but this change is challenging to see by eye due to the relative dimness of the QDs at this shell thickness and concentration. In the middle row, QDs with moderate shell thicknesses are quite bright, are visibly quenched by the peptide-dye, and QD emission visibly recovers upon enzymatic cleavage. With the thickest shelled QD donors in the bottom row of the tubes, the emissions from the QDs are very bright in all of the tubes, making discernment between the quenched and unquenched state difficult.

For quantitative analysis, 30 μL of QD, QD + peptide-dye, and QD + peptide-dye + enzyme were monitored spectroscopically over time. In this assay, the number of acceptors per donor was halved compared to the visual test and a less (0.2 nmol) enzyme was added per assay. In both assays (visual and spectroscopic), an excess of the peptide-acceptor and enzyme were used. Because FRET efficiency is highest and initial sensor PL the lowest when using the smallest QDs, the extent of QD PL enhancement from enzyme cleavage relative to a sensor + no enzyme control is highest (Fig. 4A). However, the signal intensity of the sensor using the thin-shelled QDs is so relatively dim that even after a four-fold increase in brightness following enzyme addition, the difference is difficult to see visibly. PL of thin shelled QDs can be measured with a fluorimeter, but is difficult to see by eye at low concentrations. Medium- and thick-shelled QDs are much brighter and are easily visible at lower concentrations, but require more acceptors to exhibit visible quenching (Fig. S10†).

Experimental

Materials

gQD synthesis. Cadmium oxide (CdO; 99.95%, Alfa Aesar), sulfur (99.95%, ACROS Organics), 1-octadecene (ODE; 90%, ACROS Organics), and oleylamine (80%–90%) were used as purchased from Fisher Scientific. Zinc acetate (99.99%), selenium pellets (99.99%), and oleic acid (OA; 90%) were used as purchased from Sigma-Aldrich for gQD synthesis. HPLC-grade solvents including hexanes (Fisher Scientific), methanol (Honeywell), Chloroform (J.T. Baker), and ethanol (Sigma-Aldrich) were bought and used without further purification.

Ligand reagents. DL-Thioctic acid (≥98%, ACROS Organics), 1,1′-carbonyldiimidazole (CDI, 97%, ACROS Organics), ethylenediamine (≥99%, Sigma-Aldrich), methyl acrylate (≥99%, ACROS Organics), lithium hydroxide (LiOH; ≥98%, Sigma-Aldrich), and sodium borohydride ($NaBH_4$, powder, Fisher Scientific) were used for CL4 synthesis. Purification columns

run during CL4 synthesis used silica gel sorbent (230–400 Mesh, Grade 60, Fisher Scientific).

Peptide-dye conjugates and FRET assays. Alexa Fluor® 647 C2 Maleimide was purchased from Life Technologies and bovine serum albumin powder from Fisher Scientific. Dimethylsulfoxide (DMSO; 99.5%), phosphate buffered saline, pH 7.4, α-Chymotrypsin from Bovine Pancreas, Type II, ≥40 units per mg and HEPES were purchased from Sigma-Aldrich and used for preparation of buffers and reagents for FRET assays.

Quantum dot synthesis

Precursor preparation. To prepare 0.2 M cadmium oleate ($Cd(OA)_2$), 2.57 g of CdO and 28.07 or 70.18 mL of OA was loaded into a 250 mL round bottom flask (rbf) for a Cd : OA ratio of 1 : 4 or 1 : 10, respectively. The mixture was then degassed and heated to 100 °C. The reaction was vacuumed at 100 °C until it began to clarify, at which point it was backfilled with argon and 72 or 29.89 mL of ODE was added to the flask to yield a 100 mL solution at 0.2 M $Cd(OA)_2$. Complete conversion of the CdO occurred upon heating to 180 °C under argon, as indicated by the solution turning clear. Once complete conversion has occurred, the precursor was allowed to cool to 100 °C and degassed for ~1 h to ensure complete removal of water. The precursor solution is a waxy solid at room temperature and warmed under argon to 80 °C when in use.

The 0.2 M zinc oleate ($Zn(OA)_2$) precursor was prepared with a 1 : 4 Zn : OA ratio in the same manner as $Cd(OA)_2$. Specifically, 4.39 g of zinc acetate was added to 28.05 mL of OA and converted before 71.95 mL of ODE were added to dilute the product to 0.2 M in 100 mL. The precursor solution is solid at room temperature and stored under argon at 95 °C when in use.

A 1 M TOP : Se stock was made by adding 3.95 g of selenium pellets to 50.03 mL of TOP and stirring overnight at 80 °C. 100 mL of 0.2 M precursor solution was made by diluting 20 mL of the 1 M stock to a total volume of 100 mL with 80 mL of ODE. The precursor was then stored at room temperature under argon.

A 0.2 M sulfur precursor was made by adding 1.28 g of elemental sulfur to 199.59 mL of ODE and stirred overnight at 80 °C. Sulfur precipitates from solution at room temperature and is kept at 80 °C under argon when in use.

Quantum dot core synthesis. CdSe cores were nucleated using a modified version of a previously described hot injection method.[17] 1 g TOPO, 8 mL ODE, and 10 mL of 0.2 M $Cd(OA)_2$ (1 : 4) were loaded into a 100 mL rbf and degassed at room temperature and at 80 °C for 30 min each. The solution was then heated to 300 °C at which point a pre-mixed bolus injection comprising 0.4 mL 1 M TOP : Se, 3 mL oleylamine, and 1 mL ODE solution was added to the flask. After 3 min, the rbf was removed from its heating mantle and cooled to room temperature. The solution was degassed for 45 min at room temperature. The cores were precipitated under air-free conditions using ethanol and methanol and redispersed in hexane.

Shelling reactions. 1–16 atomic monolayers of CdS were added to the CdSe core *via* a modified successive ion layer adsorption reaction (SILAR) method as reported by Ghosh, *et al.*[17] Briefly, 5 mL of ODE and 5 mL oleylamine were added to 6 different 100 mL rbfs and heated to 80 °C under vacuum for 30 min each. The amount of precursor needed to add a single atomic monolayer of shell material was calculated on a volume basis using the density and lattice constant for wurtzite CdS. The calculated amount of 0.2 M $Cd(OA)_2$ correlating to a single cation layer was added dropwise to the core solution at 160 °C and annealed for 2.5 h. After 2.5 h, the temperature of the reaction flask was raised to 240 °C and the same volume of 0.2 M sulfur precursor was injected dropwise, followed by a 1 h anneal. The anneal temperature was set to 240 °C for all subsequent cation/anion addition and anneal cycles. Each flask differed only in the number of CdS shells added to the initial core solution. Shells 1–4 were made using $Cd(OA)_2$ with a 1 : 4 ratio of Cd to OA, while shells 5 and above utilized the 1 : 10 Cd : OA $Cd(OA)_2$. The Cd additions were halted in the six flasks after 1, 4, 7, 10, 13, or 16 rounds of SILAR, respectively. After substantial samples of the core/shell heterostructures were removed, 2 layers of ZnS shell were added to each shell-thickness reaction using 0.2 M $Zn(OA)_2$ and 0.2 M sulfur in ODE and 30 min anneals at 240 °C after each injection.

Ligand synthesis. A short hydrophilic ligand, compact ligand four (CL4), developed by Susumu, *et al.*, was used to water solubilize the QDs.[53] The ligand was synthesized as previously described,[53] with the following modification: reaction volumes were increased four-fold and extra salts were removed by filtration prior to the evaporation of ethanol. For example, 12 g (0.0145 mol) of thioctic acid and 10.36 g (0.064 mol) of CDI were added to a 250 mL rbf and purged with argon. 120 mL of chloroform was added by syringe and the mixture was stirred for 1 h at room temperature under active argon flow. 32 mL of ethylene diamine and 120 mL of chloroform were loaded into a separate 1 L rbf under argon with an addition funnel attached. The thioctic acid/CDI/chloroform mixture was then added dropwise to the ethylene diamine mixture dropwise over the course of 4 h and left to stir at room temperature overnight under active argon flow. The solution was transferred to a separatory funnel and 400 mL of DI water added. The mixture was shaken and left to separate. The chloroform layer was collected and the water layer washed three additional times with chloroform. The organic layers were combined and vacuum concentrated to ~80 mL to be purified on silica gel with $CHCl_3$/MeOH (5 : 1) as eluent. The purified crude product was concentrated under vacuum to ~60 mL and diluted with 280 mL MeOH. 40 mL of methyl acrylate was added dropwise *via* addition funnel and the resulting solution was left to stir for 2 days under active argon flow at room temperature. The excess methyl acrylate and solvent was evaporated off and the product purified by silica gel with $CHCl_3$/MeOH (20 : 1) as eluent. Excess solvent was then evaporated off until a yellow oil remained. The product was weighed and stored at 4 °C for subsequent ring-opening immediately prior to QD ligand exchange.

To ring open the stored product, 20.9 mg LiOH, 2 mL EtOH and 1 mL DI H_2O was added for every 0.321 g of product. The mixture was allowed to react for 2 hours at room temperature before 4 M HCl was used to adjust the pH of the solution to ~8. For every 0.321 g of product, 60.6 mg of $NaBH_4$ was

added, and the mixture was stirred for 1.5 h under active argon flow. The pH of the solution was then adjusted to ~7–8 and filtered through a cotton plug in order to remove precipitated salts. The excess EtOH was evaporated off, resulting in a clear aqueous CL4 solution at a ~760 mM concentration.

Ligand exchange. A biphasic mixture of QDs in chloroform and 760 mM CL4 in water was left to stir overnight in argon filled glass vials. The ratio of CL4 to QD was adjusted to account for the larger surface area of gQDs such that 3500 molecules of CL4 per unit surface area (nm^2) of QD was used in each transfer. For example, 1.4 mL of 760 mM CL4 was added to 1 mL of a 3.96 μM CdSe/1CdS/2ZnS QD solution in chloroform and left to stir overnight after flushing with argon and capping. With overnight stirring, the QDs transfered to the water phase and the chloroform phase became clear. The water phase was collected, filtered through a 0.1 μm PVDF syringe filter (Celltreat Scientific Products LLC), and buffer exchanged with PBS, pH 7.4, three times using 30 kDa centrifugal filters (EMD Millipore). Ligand-exchanged QDs were stored concentrated at 4 °C.

Dye-labeling of acceptor peptide. The peptide sequence used for all FRET and enzymatic cleavage assays was ordered from and synthesized by Biomatik. The sequence used, Ac-HHHHHH-GL(Aib)AAGGWGC-NH2, was previously described by Medintz, *et al.*[43] The peptide includes six histidines for chelation to the QD surface and a chymotrypsin cleavage site separated by a generic spacer sequence. Aib refers to the synthetic amino acid alpha-aminoisobutryic acid.

A 100 μM peptide solution in 10 mM PBS, pH 7.4, was treated with a 10-fold molar excess of TCEP to reduce disulfide bonds. A freshly made 10 mM solution of Alexa Fluor® C2 Maleimide in DMSO was added dropwise to the peptide solution. The final reaction contained 800 nmol of maleimide-dye and 160 nmol of peptide. The conjugation ran overnight at 4 °C and was subsequently purified *via* Ni-NTA immobilized metal affinity chromatography (IMAC). The purified product was buffer exchanged to PBS, pH 7.4, using 3 kDa MWCO centrifugal filters (EMD Millipore) to remove excess peptide and concentrate the labeled peptide solution.

Quantum dot characterization

Transmission electron microscopy. The core, core/shell, and core/shell/shell samples were imaged on a JEOL 2100 TEM. Analysis of many transmission electron micrographs (n = 109–535) yielded the core and shell size of each QD.

Dynamic light scattering. DLS measurements were taken on a Brookhaven 90plus Nano-particle Sizer. The run time for each measurement was set for 1 min and each sample was measured 3–5 times. Reported hydrodynamic diameters were taken from the number averaged measurements using a particle refractive index of 1.6.

QD optical characterization. The initial concentration and subsequent dilution of each SILAR reaction flask was kept track of and samples of as-synthesized QDs at known concentration were stored in glass vials. Absorption measurements of as-synthesized CdSe/xCdS QDs diluted in chloroform were taken on a Nanodrop 2000c (Thermo Scientific) in cuvettes to back-calculate their molar extinction coefficients at 400 nm. This was not done for CdSe/xCdS/2ZnS QD samples due to the turbidity of the as-synthesized solutions of the samples with >10 CdS monolayers. Absorbance measurements of the CdSe/xCdS/2ZnS QDs were taken in water and then normalized to the measured molar extinction coefficient to generate the plot in Fig. 2D.

Photoluminescence was measured on a Horiba Jobin Yvon Nanolog. The relative quantum yields of each of the samples was determined by plotting integrated emission as a function of absorption at excitation wavelength (400 nm) of 3–5 sample dilutions and comparing the resulting slope to that of Rhodamine 6G (R6G) in ethanol. The quantum yield of R6G in ethanol is 94% and independent of concentration up to 20 μM when excited at 488 nm.[66] The differences in excitation wavelengths were accounted for by dividing the measured emission intensity by the lamp intensity at each wavelength. The brightness of each heterostructure was determined by multiplying the ε_{QD} at 400 nm (the excitation wavelength for the QY measurements) by the relative QY.

PL decay measurements were taken using a fluorescence lifetime spectrometer (LifeSpec II, Edinburg Instruments), employing a time-correlated single photon counting technique. Samples were excited at 405 nm using a pulse diode laser (EPL-405, Edinburg Instruments) at 2 μs pulse period. Photons were collected over a 0.5–2 μs time range with channel widths of 1.02 ns. The collected lifetimes were fit to a tri-exponential decay (F980 Software, Edinburg Instruments):

$$I(t) = A_1 e^{-\frac{t}{\tau_1}} + A_2 e^{-\frac{t}{\tau_2}} + A_3 e^{-\frac{t}{\tau_3}} \quad (1)$$

where t represents time and A_i are coefficients that indicate the weight associated with each decay time. Average amplitude weighted lifetimes were calculated using:[67]

$$\tau_{ave} = \frac{A_1\tau_1 + A_2\tau_2 + A_3\tau_3}{A_1 + A_2 + A_3} \quad (2)$$

FRET assays

The QD : AF647 FRET systems were allowed to bind *via* histidine-mediated self-assembly in PBS + 1% (w/v) BSA solution. Well plate assays were prepared in triplicate using black, non-binding 384 well-plates (Corning) such that donor to acceptor ratios (D : A) ranged from 0 to 10. QD excitation was set to 400 nm with a slit width of 2 nm and spectra was collected using the MicroMax Plate Reader attachment for the Horiba Nanolog Fluorimeter. The PL decay of QD + his-tagged AF647 solutions prepared in a similar manner was measured in cuvettes while stirring. For enzymatic cleavage assays, QD only, QD + His6 + AF647 (no FRET control), and QD + His6 : AF647 (FRET quenched sensor) wells were prepared in sextuplicate for each QD donor. PL spectra were taken before addition of enzyme. After initial measurement, 5 μL of 1 mg mL^{-1} α-chymotrypsin in 10 mM HEPES, pH 8 was added to 3 replicates while the remaining 3 were loaded with 10 μL of 10 mM HEPES, pH 8. PL was measured every 5 min over 1 h in order to monitor change in sensor brightness over time. Change in sensor brightness was calculated by normalizing the PL of the

enzyme loaded wells to that of the buffer only controls. This was then multiplied by initial FRET quenched QD PL to compare brightness between QD donors. The photo in Fig. 4A was generated by replicating the wells used in the enzyme cleavage assays in 200 μL PCR tubes. 1 nmol of enzyme was added to the rightmost tube and the photo was taken approximately 10 minutes after addition of enzyme.

FRET analysis

The overlap integral, J, describes the spectral overlap of the donor emission and acceptor absorption. Specifically:

$$J = \int \overline{F_D}(\lambda)\varepsilon_A(\lambda)\lambda^4 d\lambda \quad (3)$$

where $\overline{F_D}(\lambda)$ is the normalized emission spectrum of the donor and $\varepsilon_A(\lambda)$ is the molar extinction coefficient of the acceptor as a function of wavelength, λ. Förster distance, R_0, defined as the distance at which E_{FRET} is 50%, is a function of dipole orientation factor, κ^2, donor QY, Q_D, overlap integral, and solvent refractive index, η:

$$R_0{}^6 = (8.785 \times 10^{-5})\kappa^2 Q_D \frac{J}{\eta^4}. \quad (4)$$

The dipole orientation has been assumed to be random, so κ^2 has been set to 2/3 for all calculations.

E_{FRET} is experimentally determined by the degree of donor quenching. Raw FRET spectra were background subtracted for direct acceptor excitation and peak fitted using OriginPro. The E_{FRET} of the peak-fitted and background-subtracted data was calculated using the following expression:

$$E_{FRET} = 1 - \frac{F_{DA}}{F_D} = 1 - \frac{\tau_{DA}}{\tau_D} \quad (5)$$

where F_D and τ_D are the emission intensity and average fluorescence lifetime of the donor alone, and F_{DA} and τ_D are the emission intensity and average fluorescence lifetime of the donor in the presence of acceptor(s). F_D is normalized to the collisional quenching control at the same dye concentration in order to account for non-FRET based quenching. E_{FRET} can also be described as a function of the average number of acceptors per donor, **n**, taking into account that given a specific donor acceptor ratio, the specific number of acceptors, **k**, bound to each donor is described by a Poissonian distribution:[40,68]

$$E_{FRET}(\mathbf{n}) = \sum_{\mathbf{k}=1}^{\infty} \frac{\mathbf{n}^{\mathbf{k}} e^{-\mathbf{n}}}{\mathbf{k}!} \frac{\mathbf{k}R_0{}^6}{(\mathbf{k}R_0{}^6 + \mathbf{k}R_{DA}{}^6)} \quad (6)$$

R_{DA} was calculated from eqn (6) using the experimentally determined FRET efficiency and R_0, as calculated with eqn (4).

Conclusions

High-quality CdSe/xCdS and CdSe/xCdSe/2ZnS heterostructured QDs were synthesized and characterized to demonstrate the advantages and disadvantages of gQDs in biological applications. The thick-shelled, Zn-capped gQDs exhibit relative brightness 38-fold larger than those of thin-shelled, ZnS-capped QDs. For energy transfer, high brightness is useful in low concentration assays when enhanced signal to noise ratios is beneficial. The disadvantage of using gQD donors in FRET assays is the increased donor–acceptor distance that decreases maximum FRET efficiency. The overall QD size is minimized by using short, thiol-based ligands for water solubilization. Thin-shelled or core-only QDs are non-emissive following thiol-based bond ligand transfer, but photoluminescence can persist (albeit dimmed) when the QDs are capped by a protective layer of the high bandgap semiconductor, ZnS. QDs with more than 7 CdS MLs do not need the ZnS layer to exhibit measurable PL following ligand exchange, but quantum yields are higher for all samples with the ZnS cap. CdSe/7CdS/2ZnS QDs showed optimal properties as gQD FRET donors. They maintain the highest QY after ligand transfer with the thiol-based ligand and exhibit FRET efficiencies of up to 60% when attached to a dye-labeled peptide. Furthermore, their brightness in water is up to 8 times that of thin shelled or commercially available ITK655 QDs. A test sensor was made to monitor α-chymotrypsin proteolytic activity. The sensor exhibited a significant decrease in FRET signal as a direct consequence of peptide cleavage and demonstrated the viability of gQD donor FRET assemblies as biological sensors.

Conflicts of interest

There are no conflicts to declare.

Acknowledgements

This work was performed in part at the Center for Nanoscale Systems (CNS), a member of the National Nanotechnology Infrastructure Network (NNIN), which is supported by the National Science Foundation under NSF award no. ECS-0335765. CNS is part of Harvard University. This work was supported in part through a Boston University Materials Science and Engineering Innovation Grant. Financial support for Margaret Chern was provided through the Clare Boothe Luce (CBL) Program from the Henry Luce Foundation.

Notes and references

1 I. L. Medintz, H. T. Uyeda, E. R. Goldman and H. Mattoussi, *Nat. Mater.*, 2005, **4**, 435–446.
2 A. M. Dennis, J. B. Delehanty and I. L. Medintz, *J. Phys. Chem. Lett.*, 2016, **7**, 2139–2150.
3 A. M. Smith and S. Nie, *Acc. Chem. Res.*, 2010, **43**, 190–200.
4 Z. Deng, H. Yan and Y. Liu, *J. Am. Chem. Soc.*, 2009, **131**, 17744.
5 O. Adegoke and E. Y. Park, *Sci. Rep.*, 2016, **6**, 27288.
6 F. García-Santamaría, Y. Chen, J. Vela, R. D. Schaller, J. A. Hollingsworth and V. I. Klimov, *Nano Lett.*, 2009, **9**, 3482.

7 J. Vela, H. Htoon, Y. Chen, Y. S. Park, Y. Ghosh, P. M. Goodwin, J. H. Werner, N. P. Wells, J. L. Casson and J. A. Hollingsworth, *J. Biophotonics*, 2010, **3**, 706–717.
8 S. J. Lim, M. U. Zahid, P. Le, L. Ma, D. Entenberg, A. S. Harney, J. Condeelis and A. M. Smith, *Nat. Commun.*, 2015, **6**, 8210.
9 Y. Chen, J. Vela, H. Htoon, J. L. Casson, D. J. Werder, D. A. Bussian, V. I. Klimov and J. A. Hollingsworth, *J. Am. Chem. Soc.*, 2008, **130**, 5026.
10 M. Benoit, S. Piernicola, B. Stéphanie, Q. Xavier, H. Jean-Pierre and D. Benoit, *Nat. Mater.*, 2008, **7**, 659.
11 A. M. Dennis, B. D. Mangum, A. Piryatinski, Y.-S. Park, D. C. Hannah, J. L. Casson, D. J. Williams, R. D. Schaller, H. Htoon and J. A. Hollingsworth, *Nano Lett.*, 2012, **12**, 5545.
12 K. Kim, H. Lee, J. Ahn and S. Jeong, *Appl. Phys. Lett.*, 2012, **101**, 073107.
13 B. D. Mangum, F. Wang, A. M. Dennis, Y. Gao, X. Ma, J. A. Hollingsworth and H. Htoon, *Small*, 2014, **10**, 2892–2901.
14 D. Canneson, L. Biadala, S. Buil, X. Quelin, C. Javaux, B. Dubertret and J. P. Hermier, *Phys. Rev. B: Condens. Matter*, 2014, **89**, 035303.
15 M. Nasilowski, P. Spinicelli, G. Patriarche and B. Dubertret, *Nano Lett.*, 2015, **15**, 3953.
16 Y.-S. Park, A. V. Malko, J. Vela, Y. Chen, Y. Ghosh, F. Garcia-Santamaria, J. A. Hollingsworth, V. I. Klimov and H. Htoon, *Phys. Rev. Lett.*, 2011, **106**, 187401.
17 Y. Ghosh, B. D. Mangum, J. L. Casson, D. J. Williams, H. Htoon and J. A. Hollingsworth, *J. Am. Chem. Soc.*, 2012, **134**, 9634–9643.
18 J. Kundu, Y. Ghosh, A. M. Dennis, H. Htoon and J. A. Hollingsworth, *Nano Lett.*, 2012, **12**, 3031–3037.
19 A. M. Keller, Y. Ghosh, M. S. Devore, M. E. Phipps, M. H. Stewart, B. S. Wilson, D. S. Lidke, J. A. Hollingsworth and J. H. Werner, *Adv. Funct. Mater.*, 2014, **24**, 4796–4803.
20 X. Peng, M. C. Schlamp, A. Kadavanich and A. P. Alivisatos, *J. Am. Chem. Soc.*, 1997, **119**, 7019–7029.
21 J. van Embden, J. Jasieniak and P. Mulvaney, *J. Am. Chem. Soc.*, 2009, **131**, 14299.
22 F. Garcia-Santamaria, S. Brovelli, R. Viswanatha, J. A. Hollingsworth, H. Htoon, S. A. Crooker and V. I. Klimov, *Nano Lett.*, 2011, **11**, 687–693.
23 J. R. Lakowicz, *Principles of fluorescence spectroscopy*, Springer, New York, 3rd edn, 2006.
24 I. Medintz and N. Hildebrandt, *FRET - Förster resonance energy transfer: from theory to applications*, Wiley-VCH, 2014.
25 M. Stewart, A. Huston, A. Scott, E. Oh, W. Algar, J. Deschamps, K. Susumu, V. Jain, D. Prasuhn, J. Blanco-Canosa, P. Dawson and I. Medintz, *ACS Nano*, 2013, **7**, 9489.
26 S. Huang, H. Qiu, Q. Xiao, C. S. Huang, W. Su and B. Hu, *J. Fluoresc.*, 2013, **23**, 1089–1098.
27 I. L. Medintz and H. Mattoussi, *Phys. Chem. Chem. Phys.*, 2008, **11**, 17–45.
28 D. E. Prasuhn, A. Feltz, J. B. Blanco-Canosa, K. Susumu, M. H. Stewart, B. C. Mei, A. V. Yakovlev, C. Loukov, J.-M. Mallet, M. Oheim, P. E. Dawson and I. L. Medintz, *ACS Nano*, 2010, **4**, 5487.
29 A. R. Clapp, I. L. Medintz, J. M. Mauro, B. R. Fisher, M. G. Bawendi and H. Mattoussi, *J. Am. Chem. Soc.*, 2004, **126**, 301.
30 A. Shamirian, A. Ghai and P. Snee, *Sensors*, 2015, **15**, 13028–13051.
31 R. Alam, D. M. Fontaine, B. R. Branchini and M. M. Maye, *Nano Lett.*, 2012, **12**, 3251.
32 R. Alam, J. Zylstra, D. M. Fontaine, B. R. Branchini and M. M. Maye, *Nanoscale*, 2013, **5**, 5303–5306.
33 R. Alam, L. M. Karam, T. L. Doane, J. Zylstra, D. M. Fontaine, B. R. Branchini and M. M. Maye, *Nanotechnology*, 2014, **25**, 495606.
34 W. R. Algar, D. Wegner, A. L. Huston, J. B. Blanco-Canosa, M. H. Stewart, A. Armstrong, P. E. Dawson, N. Hildebrandt and I. L. Medintz, *J. Am. Chem. Soc.*, 2012, **134**, 1876.
35 H. S. Afsari, M. Cardoso Dos Santos, S. Lindén, T. Chen, X. Qiu, P. M. P. van Bergen en Henegouwen, T. L. Jennings, K. Susumu, I. L. Medintz, N. Hildebrandt and L. W. Miller, *Sci. Adv.*, 2016, **2**, e1600265.
36 M. Suzuki, Y. Husimi, H. Komatsu, K. Suzuki and K. T. Douglas, *J. Am. Chem. Soc.*, 2008, **130**, 5720.
37 A. M. Dennis, W. J. Rhee, D. Sotto, S. N. Dublin and G. Bao, *ACS Nano*, 2012, **6**, 2917.
38 P. T. Snee, R. C. Somers, G. Nair, J. P. Zimmer, M. G. Bawendi and D. G. Nocera, *J. Am. Chem. Soc.*, 2006, **128**, 13320.
39 A. Shamirian, H. Samareh Afsari, A. Hassan, L. W. Miller and P. T. Snee, *ACS Sens.*, 2016, **1**, 1244–1250.
40 W. R. Algar, M. G. Ancona, A. P. Malanoski, K. Susumu and I. L. Medintz, *ACS Nano*, 2012, **6**, 11044–11058.
41 M. Massey, J. J. Li and W. R. Algar, in *Cancer Nanotechnology: Methods and Protocols*, ed. R. Zeineldin, Springer New York, New York, NY, 2017, pp. 63–97, DOI: 10.1007/978-1-4939-6646-2_4.
42 W. R. Algar, A. Malonoski, J. R. Deschamps, J. B. Blanco-Canosa, K. Susumu, M. H. Stewart, B. J. Johnson, P. E. Dawson and I. L. Medintz, *Nano Lett.*, 2012, **12**, 3793–3802.
43 I. L. Medintz, A. R. Clapp, F. M. Brunel, T. Tiefenbrunn, H. T. Uyeda, E. L. Chang, J. R. Deschamps, P. E. Dawson and H. Mattoussi, *Nat. Mater.*, 2006, **5**, 581–589.
44 K. Boeneman, B. C. Mei, A. M. Dennis, G. Bao, J. R. Deschamps, H. Mattoussi and I. L. Medintz, *J. Am. Chem. Soc.*, 2009, **131**, 3828.
45 S. Thiollet, C. Bessant and S. L. Morgan, *Anal. Biochem.*, 2011, **414**, 23.
46 H. Peng, L. Zhang, T. H. M. Kjällman, C. Soeller and J. Travas-Sejdic, *J. Am. Chem. Soc.*, 2007, **129**, 3048.
47 X. Qiu, J. Guo, Z. Jin, I. L. Medintz and N. Hildebrandt, *Small*, 2017, 1700332, DOI: 10.1002/smll.201700332.
48 J. Lee, M. B. Brennan, R. Wilton, C. E. Rowland, E. A. Rozhkova, S. Forrester, D. C. Hannah, J. Carlson,

E. V. Shevchenko, D. S. Schabacker and R. D. Schaller, *Nano Lett.*, 2015, **15**, 7161–7167.
49 E. R. Goldman, I. L. Medintz, J. L. Whitley, A. Hayhurst, A. R. Clapp, H. T. Uyeda, J. R. Deschamps, M. E. Lassman and H. Mattoussi, *J. Am. Chem. Soc.*, 2005, **127**, 6744.
50 S. Bhuckory, O. Lefebvre, X. Qiu, K. D. Wegner and N. Hildebrandt, *Sensors*, 2016, **16**, 197.
51 X. Qiu, K. D. Wegner, Y.-T. Wu, P. M. P. van Bergen En Henegouwen, T. L. Jennings and N. Hildebrandt, *Chem. Mater.*, 2016, **28**, 8256.
52 J. J. Li, Y. A. Wang, W. Guo, J. C. Keay, T. D. Mishima, M. B. Johnson and X. Peng, *J. Am. Chem. Soc.*, 2003, **125**, 12567.
53 K. Susumu, E. Oh, J. B. Delehanty, J. B. Blanco-Canosa, B. J. Johnson, V. Jain, W. J. T. Hervey, W. R. Algar, K. Boeneman, P. E. Dawson and I. L. Medintz, *J. Am. Chem. Soc.*, 2011, **133**, 9480–9496.
54 A. M. Dennis, D. C. Sotto, B. C. Mei, I. L. Medintz, H. Mattoussi and G. Bao, *Bioconjugate Chem.*, 2010, **21**, 1160–1170.
55 P. Reiss, M. Protiere and L. Li, *Small*, 2009, **5**, 154–168.
56 H. T. Uyeda, I. L. Medintz, J. K. Jaiswal, S. M. Simon and H. Mattoussi, *J. Am. Chem. Soc.*, 2005, **127**, 3870–3878.
57 E. Cai, P. Ge, S. H. Lee, O. Jeyifous, Y. Wang, Y. Liu, K. M. Wilson, S. J. Lim, M. A. Baird, J. E. Stone, K. Y. Lee, M. W. Davidson, H. J. Chung, K. Schulten, A. M. Smith, W. N. Green and P. R. Selvin, *Angew. Chem., Int. Ed.*, 2014, **53**, 12484–12488.
58 G. Palui, T. Avellini, N. Zhan, F. Pan, D. Gray, I. Alabugin and H. Mattoussi, *J. Am. Chem. Soc.*, 2012, **134**, 16370–16378.
59 D. Reddy, D. Kim, S. Rhee, B. Lee and C. Liu, *Nanoscale Res. Lett.*, 2014, **9**, 1–8.
60 D. Shepherd, K. Whitcomb, K. Milligan, P. Goodwin, M. P. Gelfand and A. Van Orden, *J. Phys. Chem. C*, 2010, **114**, 14831–14837.
61 A. Clapp, E. Goldman and H. Mattoussi, *Nat. Protoc.*, 2006, **1**, 1258–1266.
62 K. Boeneman, J. R. Deschamps, S. Buckhout-White, D. E. Prasuhn, J. B. Blanco-Canosa, P. E. Dawson, M. H. Stewart, K. Susumu, E. R. Goldman, M. Ancona and I. L. Medintz, *ACS Nano*, 2010, **4**, 7253.
63 D. J. Desilets, P. T. Kissinger and F. E. Lytle, *Anal. Chem.*, 1987, **59**, 1244–1246.
64 H. D. Heck, *J. Am. Chem. Soc.*, 1971, **93**, 23–29.
65 A. Nagy, K. Gemmill, J. Delehanty, I. Medintz and K. Sapsford, *IEEE J. Sel. Top. Quantum Electron.*, 2014, **20**, 115–126.
66 M. Fischer and J. Georges, *Chem. Phys. Lett.*, 1996, **260**, 115–118.
67 I. L. Medintz, T. Pons, K. Susumu, K. Boeneman, A. Dennis, D. Farrell, J. R. Deschamps, J. S. Melinger, G. Bao and H. Mattoussi, *J. Phys. Chem. C*, 2009, **113**, 18552–18561.
68 T. Pons, I. L. Medintz, X. Wang, D. S. English and H. Mattoussi, *J. Am. Chem. Soc.*, 2006, **128**, 15324.